Surface & Coatings Technology 357 (2019) 353–363

Contents lists available at ScienceDirect

Surface & Coatings Technology

journal homepage: www.elsevier.com/locate/surfcoat

The tin stabilization effect on the microstructure, corrosion and wear resistance of electroless NiB coatings

L. Bonin*, V. Vitry, F. Delaunois

Metallurgy Lab, UMONS, 20 place du Parc, 7000 Mons, Belgium

ARTICLE INFO

Keywords:
Electroless plating
Nickel-boron
Stabilizer
Tin

ABSTRACT

The effect of tin chloride on bath stabilization and properties of electroless Nickel-Boron (NiB) coatings was investigated. NiB coatings were synthesized by electroless deposition using $SnCl_2$ stabilizer. Sn was codeposited in the coating generating a novel NiB-Sn alloy. The deposition of NiB-Sn occurred in an aqueous bath containing a reducible metal salt ($NiCl_2$), reducing agent ($NaBH_4$) and complexing agent ($C_2H_4(NH_2)_2$). The pH was controlled at pH 12 ± 1 in order to avoid bath destabilization. The stabilizer properties of $SnCl_2$ were proved by the fact that the plating completely stops at high concentrations. It has been found in the present work that the $SnCl_2$ not only stabilizes electroless nickel baths but also enhances the plating rate. The deposition was performed with three different concentrations of $SnCl_2$ (0.05 g/L, 0.1 g/L and 0.2 g/L). The morphological features are modified as a function of concentration. Coatings with finer cauliflower structure and more homogeneous thickness are reached with the increase of stabilizer concentration. The corrosion behavior was increased with the Sn presence in the surface. Results for samples with 0.1 g/L of $SnCl_2$ show hardness (842 hk_{50}) wear behavior (Ws 0.11 $\mu m^2/N$) and first damage by scratch test (Lc 30 N) results comparable to those presented by traditional NiB coatings.

1. Introduction

Electroless Ni plating is the autocatalytic deposition of a pure Ni or Ni alloy from an aqueous solution onto a substrate without the application of electric current; which distinguishes it from the conventional electroplating processes [1–5]. The process of electroless plating is well known and can deposit metals, alloys and composites coatings on a variety of conductive and non-conductive substrates.

Electroless nickel deposition processes are divided in three groups: NiP, NiB and pure Ni. The coatings are generated by respectively choosing the following reducing agents: hypophosphite [6–10], borohydride [11–15] (or dimethylamine borane [16–18]) and hydrazine [19,20]. Hypophosphite-reduced electroless nickel plating (NiP) has the most extensive industrial success because of its low cost, process stability and high corrosion protection [7].

Electroless NiB coatings are classified into two types, borohydride reduced and dimethylamine borane (DMAB)-reduced electroless nickel. The boron content of the deposit and the plating rate are function of the reducing agent. Usually, electroless NiB deposits reduced by (DMAB) have less than 5 wt% boron, are crystalline in nature and exhibit a low plating rate, around 6 to 9 μm/h. They are normally prepared from acidic baths at temperatures of the order of 50 °C [4,16]. Electroless NiB deposits reduced by borohydride have a boron content between 5 and 9 wt%, are amorphous in nature and exhibit a high plating rate, around 15 to 19 μm/h. They are always prepared from alkaline baths at temperatures of the order of 95 °C [21–23]. Due the high boron concentration, NiB coatings reduced by borohydride have superior hardness and mechanical properties that are comparable with hard chromium coatings and can replace these hard coatings in some applications [24,25].

Considering that electroless nickel baths are sensitive to impurities, the maintenance of the bath stability is mandatory. The addition of a stabilizer warrants a plating bath without decomposition. In particular, the stabilization mechanism is an essential element for ensuring that the plating system is free of colloidal Ni particles [26,27].

Stabilizers are chemical agents and different compounds have been identified as effective stabilizers for electroless nickel deposition [26,28–30]. In the specific case of electroless NiB coatings reduced by borohydride, stabilizers come from the heavy metal cations group. Indeed, the majority of the NiB coatings produced in laboratories and also in industry are stabilized by lead or thallium cations [23,31,32]. Tin in the state of Sn^{2+} is cited by different authors as a possible stabilizer, although baths stabilized with this component have not yet been developed [1,33,34].

The stabilizing mechanism of heavy metal ions such as Pb^{2+}, Tl^{3+}, Sn^{2+} proposes that when heavy metals are added to the plating bath,

---

* Corresponding author.
E-mail address: Luiza.bonin@umons.ac.be (L. Bonin).

https://doi.org/10.1016/j.surfcoat.2018.10.011
Received 17 August 2018; Received in revised form 26 September 2018; Accepted 3 October 2018

they deposit on the active metal surface through displacement reaction, thus inhibiting the occurrence of the random reduction of nickel [29,35]. As this stabilization process is based on the displacement reaction, stabilizer elements are also deposited in the coating generating a three-element alloy. While the lead stabilized coatings present a lead content between 0.5 and 1.5 wt% [21,32], the thallium content in some coatings reaches 8 wt% [28].

In this work, electroless NiB coatings reduced by borohydride and stabilized by tin cations were studied in a high pH solution. Tin was been used in electroless NiP coatings with the aim of improving the corrosion properties of these alloys, but stability behavior has not been observed [36,37]. Tin stabilized coatings can replace traditional lead and thallium chemistry for several applications. In addition, these new bath compositions meet the ELV 2000/53/EC [38] and the RoHS 2002/95/EC [39] compliance. First, the stabilizing capacity of tin chloride was characterized. The plating bath composition was then optimized to generate high plating rate in a stable bath. Different concentrations of Sn are used with the interest of design new coatings morphology and properties. The coatings morphology, composition, mechanical and corrosion properties for three different compositions are presented here.

2. Materials and methods

2.1. Electroless NiB bath

Mild steel (St 37) specimens with a size of 25 mm × 50 mm × 1 mm were used as the substrate material for the deposition of the electroless NiB coatings. Rectangular shaped specimens were prepared very carefully for the deposition. The samples were subjected to surface grinding process up to 1200 grade SiC paper. The samples were cleaned with acetone to remove foreign matter and corrosion products. Next, the surface of the mild steel specimens was cleaned using distilled water. After thorough cleaning, the specimens were subjected to a pickling treatment with 35% hydrochloric acid for three minutes. Subsequently, they were rinsed with flowing distilled water and directly immersed in the bath. The bath composition for electroless NiB is based on the composition developed by Delaunois et al. [40], where sodium borohydride ($NaBH_4$–99.9%) was used as reducing agent, nickel chloride hexahydrate ($NiCl_2.6H_2O$ - 99%) as nickel source, ethylenediamine (NH_2–CH_2—CH_2—NH_2 - 99%) as complexing agent, sodium hydroxide (NaOH) as pH regulator. In the original baths, lead tungstate is used as stabilizer. In the present work, the stabilization effect of tin chloride ($SnCl_2$–99.9%) at different concentrations is tested. The concentration of all the components used in the baths was kept fixed, with the exception of the stabilizer. Deposition time was kept constant (1 h). After the deposition, the samples were taken out of the electroless nickel bath, washed in distilled water and dried in air. The temperature (95 ± 1 °C) and agitation (300 rpm) were regulated by a hot plate with magnetic stirring.

The bath composition for electroless NiB-Sn coating was selected on the basis of the results of several experiments that are described in this paper. Table 1 indicates the electroless bath compositions and operating conditions used for the deposition of electroless NiB-Sn coatings.

Table 1
NiB-Sn bath composition and parameters.

NiB-Sn	TcA	TcB	TcC
Nickel chloride	24 g/L		
Sodium hydroxide	39 g/L		
Ethylenediamine	60 mL/L		
Tin chloride	0.05 g/L	0.10 g/L	0.20 g/L
Sodium borohydride	0.602 g/L		
Bath temperature	95 ± 1 °C		
Bath pH	12.5		
Plating time	1 h		

2.2. Measurement of deposition rate

The deposition rate test was used to determine the effect of the stabilizer on the plating rate, for different concentrations. 1 L of the plating solution described above with different stabilizer concentrations and mild steel specimens with a total area of 25 cm^2 were used. The samples were weighed, before and after deposition, on an analytical balance with a precision of 0.1 mg. The deposition rate R (μm/h) was calculated assuming 8.3 g/cm^3 as the density of NiB alloy (it corresponds to the density of an alloy with a B content of approximately 6%) [41].

2.3. Bath stability test

The stability test was employed to determine the effect of stabilizer concentration on the bath life time. This test was conducted with a volume of solution of 250 mL, with the same composition described above and different concentrations of stabilizer. The time starts to be recorded when the solution reaches 95 °C and all the components are in the bath. The time required for the solution to start to destabilize is recorded. The end point, or the onset of bath decomposition, was defined as the time in which the first dark precipitates emerge in the solution.

2.4. Coatings characterization methods

Surface morphology and cross-section analysis of the electroless nickel coatings was done by Scanning Electron Microscopy (SEM) (Hitachi SU8020), the cross-section morphology was analyzed after polishing with silicon carbide paper and diamond paste up to mirror finish. The elemental composition and the depth profiles of electroless nickel coatings were determined by Glow-discharge Optical Emission Spectroscopy (GDOES) using a calibrated HORIBA Jobin Yvon GD-Profiler 2.

Roughness measurement was carried out using a stylus-type profilometer, Zeiss 119 SURFCOM 1400D-3DF. The profilometer was set to a cut-off length of 0.8 mm, Gaussian filter and 20 mm evaluation length. The microdurometer Mitutoyo HM-200 equipped with a Vickers indenter loaded with 50 gf and applied for 20 s was used to determine the surface coatings hardness. The same device equipped with a Knoop indenter also loaded with 50 gf and applied for 20 s was used to determine the cross section hardness. Samples were submitted to scratch tests using the continuous increase load method. The apparatus used for this study was a CSEM scratch tester with a load rate of 100 $N{\cdot}min^{-1}$ and an advance rate of 6.75 $mm{\cdot}min^{-1}$. The final load of the test was 150 N, resulting in a scratch of 10 mm. The tip was a diamond Rockwell stylus with a radius of 200 μm. The resulting scratches were observed using a Hirox KH-8700 3d microscope.

Tribological behavior was investigated using pin-on-disk CSM microtribometers (without lubricant). The samples served as the disks and the counterparts (pins) were 6 mm diameter alumina balls (1400 HV). The sliding speed, sliding distance and normal load, were respectively, 10 cm/s, 100 m and 5 N. The specific wear rate (Ws) was calculated following the European standard EN 1017-13:2008. Where Ws is the volume wear loss ΔV divided by the applied load F_N and the sliding distance S. The digital optical microscope Hirox KH-8700 was used for the surface observations made in the context of the surface analyses. Additionally, salt spray tests were realized in a Q-FOG Cyclic corrosion tester, the samples were suspended in a cabinet and exposed to a 50 g/L ± 5 g/L NaCl solution. The air pressure of the atomized saline solution was maintained in the range of 6–8 Bar. Salt spray was carried out according to ISO 9227 standard. The tests were conducted for a variety of time periods ranging from 0.5 h to 10 days with intermediate

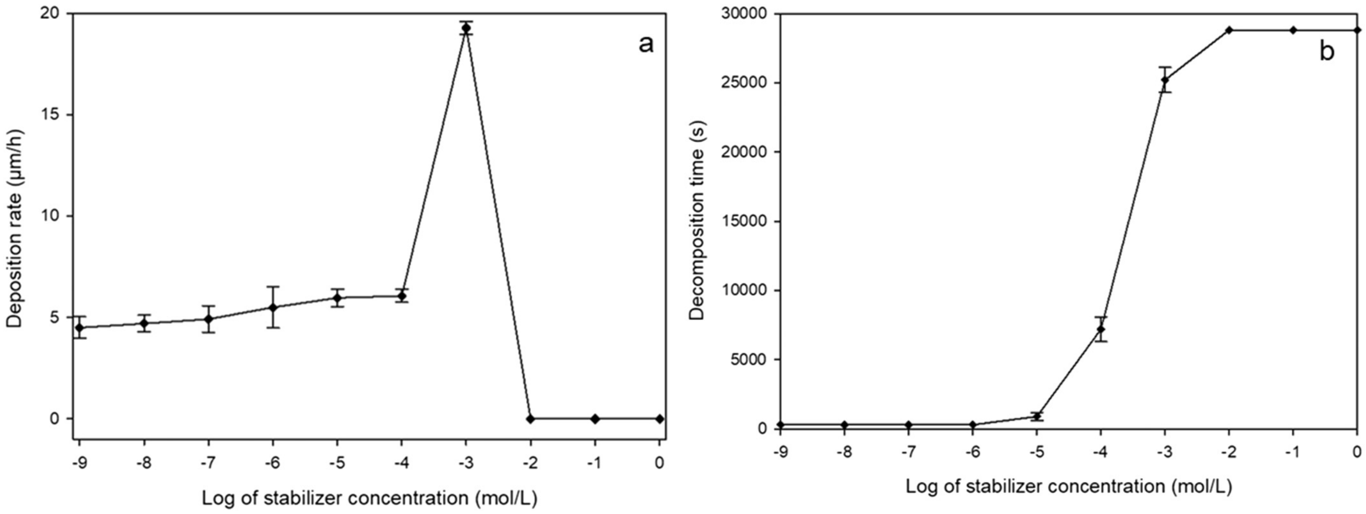

Fig. 1. (a) Effect of tin chloride concentration on deposition rate of electroless nickel, (b) Effect of tin chloride concentration on the bath life of electroless nickel.

periods of 1 h, 4 h, 8 h and 1, 2, 3, 4, 5, 7 days.

3. Experimental results and discussion

3.1. Bath stability

Sn(II) stabilizing properties were determined using the plating rate generated by different concentrations of tin chloride. This test is based on the fact that stabilizers are chemical compounds used in electroless plating in order to avoid the decomposition of the solution. The addition of these compounds to the plating solution assures the deposition under proper conditions, increasing the plating rate on the substrate. On the contrary, stabilizers are also known as inhibitors, as an increase in the concentration of stabilizers may completely inhibit the deposition reaction [1,4]. In the case of elements with significant stabilization properties, the deposition should completely stop (plating rate equals to zero) for high stabilizer concentrations. On the other hand, elements that never stop the deposition are considered as not having any stabilizing properties [42].

Deposition rate versus concentration of tin chloride is presented in Fig. 1(a). Tin chloride ($SnCl_2$) concentration in the solution varied in the range from 10^{-9} to 1 mol/L. In the range between 10^{-9} and 10^{-4} mol/L, the deposition rate is almost not influenced by the stabilizer concentration. Up to a concentration of 10^{-5} mol/L, the bath reacts like a bath without stabilizer: the deposition takes place on the substrate but nickel colloidal particles are also formed in the solution. At a concentration of 10^{-4} mol/L, the bath starts to be stabilized, the presence of nickel colloidal particles decreases and the plating is more uniform. However, these changes do not affect the plating rate, as this is based on the weight gain. The plating rate increases a lot for a concentration of 10^{-3} mol/L, reaching 19 μm/h. This stabilizer concentration generates a completely stabilized bath, as the nickel deposition occurs exclusively on the substrate and the presence of nickel colloidal particles is not observed. For concentrations of tin chloride higher or equal to 10^{-2} mol/L, the complete inhibition of plating (plating rate of 0 μm/h) is reached. The complete inhibition of plating at high concentrations of Sn(II) is attributed to the absence of catalytic sites on the substrate surface due to adsorption of tin atoms, limiting the catalytic reactions and consequently the deposition. These outcomes show that Sn(II) has stabilizer properties in the present NiB electroless plating bath. A progressive increase in the rate of nickel deposition followed by a decrease is consistent with the results observed in the literature [27,42].

The deposition rate test showed that tin chloride has stabilizer properties in the proposed NiB bath. However, as stabilizers are compounds used to avoid the decomposition of the solution assuring operations over an extended period of time, the study of the decomposition time should also be realized. The bath stability test (Fig. 1(b)) shows a significant increase in the bath life time (decomposition time) with the addition of Sn(II). The bath life increased from 300 s to 900 s as the stabilizer concentration was increased from 10^{-9} mol/L to 10^{-5} mol/L. For stabilizer concentrations equal to 10^{-4} mol/L, bath decomposition was observed after 7200 s, while for concentrations equal to 10^{-3} mol/L, the first signals of destabilization appeared after 25,200 s (7 h). Considering concentrations of tin chloride higher or equal to 10^{-2} mol/L, the baths did not present signals of decomposition until 28,800 s (8 h) and the tests were stopped after that time because such high concentrations in tin chloride completely inhibit plating. The bath stability test results show that Sn(II) has stabilizer properties for the present NiB electroless plating bath and can provide stability for extended periods of time. A progressive increase in the time until decomposition was expected as the increase in Sn(II) species decreases the catalytic activity.

The deposition rate and the bath stability tests showed a huge variation in the range between 10^{-5} to 10^{-2} mol/L. For this reason, these tests were repeated in this range with a smaller interval between the successive points. For a better interpretation, in Fig. 2(a, b), the concentration is presented in g/L and not mol/L, where 10^{-5} mol/L is equal to 0.0018 g/L and 10^{-2} mol/L is equal to 1.8 g/L.

The deposition rate test showed an impressive increase in the plating rate (6.01 to 14.46 μm/h) in the concentration range between 0.0018 and 0.05 g/L. The plating rate was 18.25 μm/h for the concentration of 0.1 g/L and reached a maximum for the concentration of 0.2 g/L, where the plating rate attains 20.84 μm/h. When the concentrations were increased to 0.3 g/L, the plating rate dropped to 2.01 μm/h. For concentrations higher or equal to 0.5, the deposition was completely stopped. The bath stability test shows an impressive increase in the bath life (from 900 to 21,600 s) in the interval between 0.0018 and 0.05 g/L. At a concentration of 0.1 g/L, the decomposition time is equal to 25,200 s (7 h), while it is equal to 27,000 s (7.5 h) for a concentration of 0.2 g/L. When the concentration is equal or higher than 0.3 g/L, the baths did not present signs of decomposition until 28,800 s (8 h) and the test was stopped after it because baths with such high concentrations did not present considerable deposition in the plating rate test.

The bath stability and plating rate test shows that Sn(II) has stabilizer properties for the present NiB, being able to provide stability for extended period of time. The next section presents the characterization of coatings generated using three different concentrations of tin chloride chosen in the range where deposition rate is the highest:

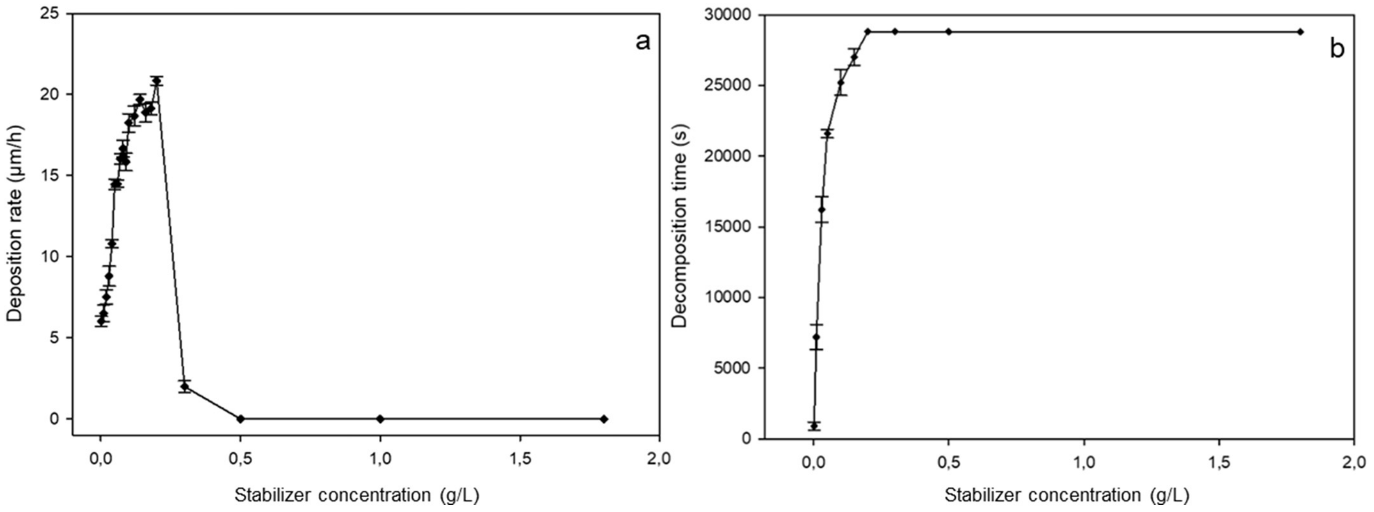

Fig. 2. (a) Effect of tin chloride concentration on the deposition rate of electroless nickel, (b) Effect of tin chloride concentration on the bath life of electroless nickel, for concentrations between 0.0018 g/L and 1.8 g/L (10^{-5} to 10^{-2} mol/L).

0.05 g/L, 0.10 g/L and 0.20 g/L.

3.2. Coatings characterization

3.2.1. Chemical and morphological characterization

This section presents the characterization of NiB-Sn coatings obtained with three different concentrations of tin chloride (Table 1).

Fig. 3 presents the depth profile chemical analysis, obtained by Glow-discharge Optical Emission Spectroscopy (GDOES). As expected, sample (a), made with 0.05 g/L of $SnCl_2$ presents the smallest concentration of Sn in the coating. At the beginning of deposition, close to the substrate, the Sn concentration is close to 1.0 wt% and it decreases linearly toward the top surface (with final values close to 0.1 wt%). The same phenomenon is shown for the boron concentration, at the beginning of deposition, the B concentration is close to 8.5 wt%, decreasing to around 6.9 wt% close to the surface. Sample (b), made with 0.1 g/L $SnCl_2$ also presents a variation in the Sn and B concentrations. The Sn concentration is close to 1.3 wt% at the beginning of the deposition and decreases to 0.5 wt% at the sample surface; while the boron content decreases from 7.6 wt% to 6.6 wt%. In the case of sample (c) (0.2 g/L $SnCl_2$), the Sn concentration in the bath is sufficient to generate a constant Sn concentration in the deposit (2.0 wt%). As a consequence, the deposition of B is almost constant, varying from 6.9 wt% at the bottom to 6.4 wt% on the surface.

Fig. 4 presents the cross section observations by SEM. Sample (a) presents morphological variations between the outer and the inner part of the film. The thickness of the coating is about 14.5 µm (for 1 h of plating). Only the inner part, closer to the substrate, with a thickness of approximately 2 µm, presents a columnar morphology as is typically observed for electroless NiB coatings. However, the outer part shows a different morphology, with the presence of features that look like trees. The morphological variation was generated by changes in the growth mode during the plating process, which is linked to the action of the stabilizer. Heavy metal ions, such as Sn^{2+}, stabilize the plating bath by depositing on the active metal surface through displacement reaction and thus inhibiting the occurrence of the random reduction of nickel [29]. This displacement reaction is more intense in the first moments of deposition because it happens initially between Fe and Sn. The presence of Sn adsorbed on the steel surface limits the lateral growth of Ni, resulting in a columnar deposit. However, as can be seen on Fig. 3(a), the Sn concentration decreases with the deposition time, making it possible for Ni to grow laterally. The columnar structure is typically observed for electroless NiB coatings [43,44], however this tree-like structure has never been described in the literature before.

Sample (b) has a cross section morphology that reminds of sample (a), but which is more uniform. The thickness of the coating is about 18.3 µm (for 1 h of plating). In this case, different growth modes are also observed. In the first 1 µm, a columnar structure can be observed. However, with the decrease of Sn concentration (Fig. 3(b)), the nickel growth is not limited laterally and the tree-like structure is revealed. In the case of this sample, the structure is more uniform, the trees are organized in columns and the space between these tree-like features is constant. This fact could be explained by the higher concentration of Sn when compared to sample (a).

The stabilizer concentration has affected the plating rate of deposits, samples with superior concentration of stabilizer showed an increase in the plating rate. This fact can be explained because some stabilizers are also activators in solution. In that case, stabilizers are responsible by an increase in the reduction efficiency of the reducing agent [45]. Consequently, the increases of stabilizers increase the plating rate and also the relation Ni/B concentration, as can be observed in the Fig. 3.

Sample (c) presents a more homogeneous cross section morphology. The thickness of the coating is about 20.8 µm (for 1 h of plating). The columnar structure is quite fine and is not well revealed by the etching process. This homogeneity can be directly correlated with the Sn concentration in the coating that stays stable throughout the coating (Fig. 3(c)). In this sample, the Sn concentration in the bath was higher and generated a uniform coating.

The surface morphology of the different deposits is presented on Fig. 5. Due to the absence of columnar structure in the outer parts of the coating, sample (a) presents a planar structure with the presence of nodules. Sample (b) presents a cauliflower like structure – similar to the typical aspect of NiB coatings [11,12,14,46]. However, the structure is slightly rougher in this case. Sample (c) has a fine cauliflower like structure, generated by the fine columns present in the cross section.

3.2.2. Mechanical and tribological properties

The average values of the superficial roughness for all the samples are shown in Table 2. The parameters chosen to represent the roughness in this study are Ra, Rv and Rp. The lowest Ra value was obtained for the TcC coating and the TcA coatings presented higher roughness. This is probably due to the better stabilization observed for higher tin concentrations (sample TcC): the more stable samples presented more uniform coatings. In addition, in the case of high stabilization, the formation of colloidal nickel outside the sample would be less important. In the case of a less stable bath, some particles could be formed outside the sample surface and adsorb to the surface afterwards, generating a rougher coating [30]. Furthermore, the Rp value is

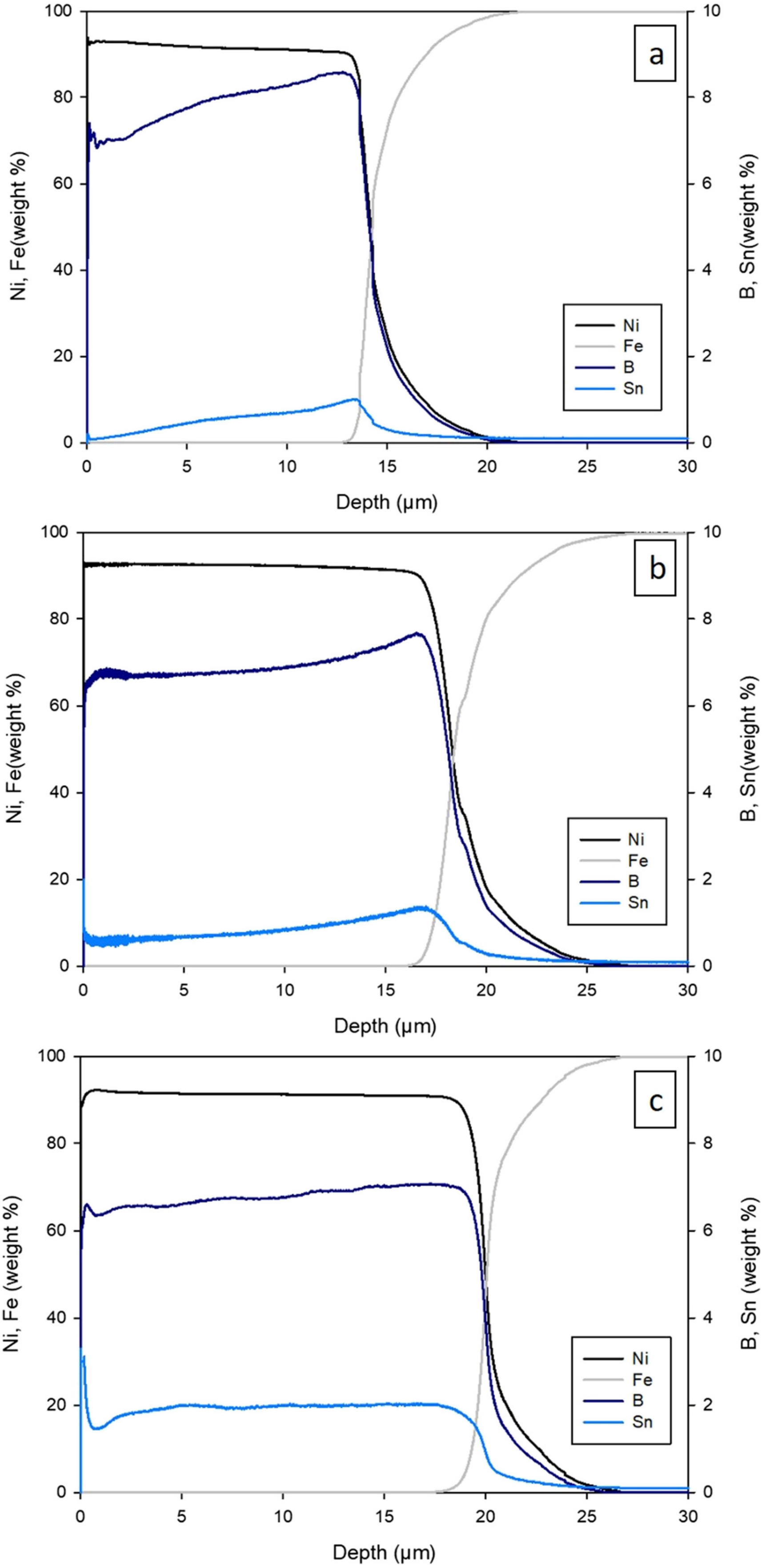

Fig. 3. Depth profile chemical analysis of electroless NiB-Sn coatings. (a) TcA, (b) TcB and (c) TcC.

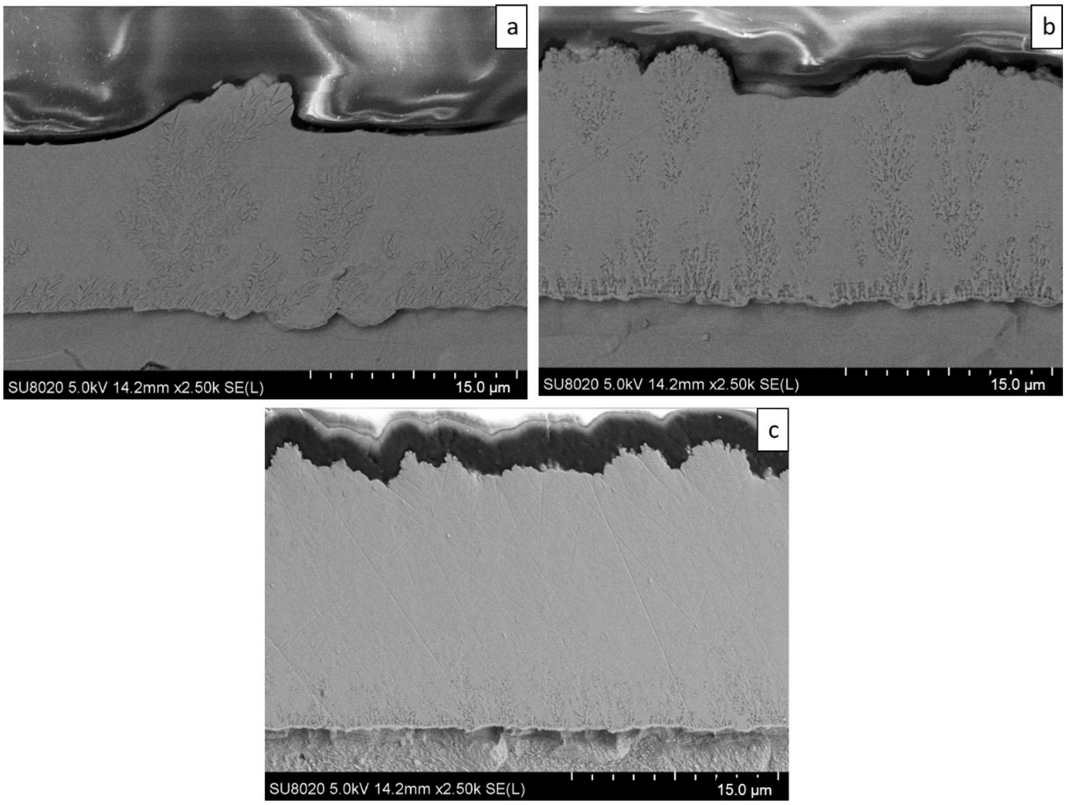

Fig. 4. Cross-section morphology of NiB-Bi samples: (a) TcA, (b) TcB and (c) TcC.

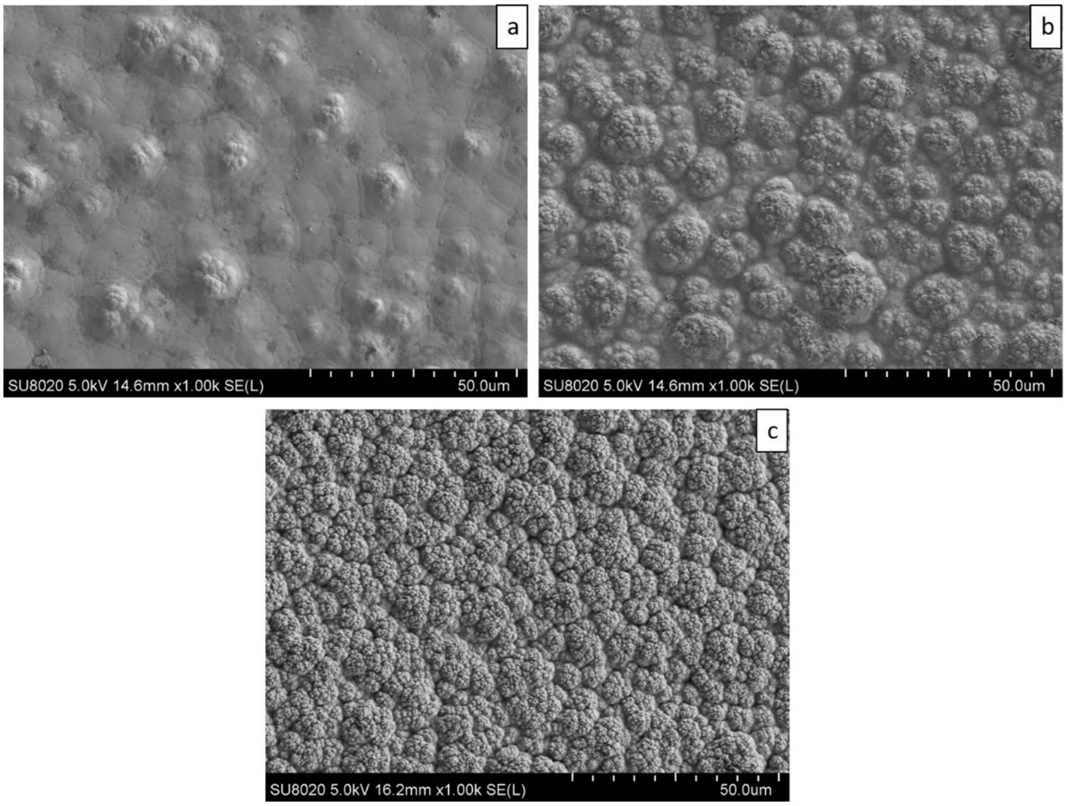

Fig. 5. Surface morphology of NiB-Sn samples; (a) TcA, (b) TcB and (c) TcC.

Table 2
Mechanical properties of the electroless nickel boron stabilized by Sn coatings.

	TcA	TcB	TcC
Vickers hardness hv (50)	555 ± 53	794 ± 61	813 ± 32
Knoop hardness hk (50)	668 ± 17	842 ± 31	867 ± 13
Roughness – Ra (μm)	0.93 ± 0.08	0.62 + 0.03	0.39 ± 0.03
Roughness – Rp (μm)	6.51 ± 0.72	2.90 + 0.29	1.41 ± 0.29
Roughness – Rv (μm)	2.23 ± 0.27	1.56 + 0.16	1.52 ± 0.24
Specific wear rate Ws (μm^2/N)	0.81	0.11	1.29
Friction coefficient μ	0.42	0.35	0.51
First damage (Lc)	28 N	30 N	18 N

considerably higher for the TcA sample (6.51 μm), which suggests a less regular coating. It is interesting to note that the Ra values of all the TcC systems stay close to that of NiB-Pb coatings (around 0.3 μm) [32,47].

Standard Vickers and Knoop hardness tests were conducted, with a load of 50 gf, on the samples surface and cross section respectively. The average hardness of 10 measurements is shown in Table 2. The systems coated with electroless NiB-Pb are much harder than those protected with NiP and this is one of the most important properties of those coatings [48]. Samples TcB and TcC presented similar resistance to permanent deformation by Vickers and Knoop indentation. Moreover, the hardness presented by these two samples is in the same range as the impressive NiB-Pb coatings [22,49–51]. The lower hardness presented by TcA sample may be due to the microstructure of the coating: as shown in the cross section (Fig. 4), this coating is formed by coarse randomly placed trees, this tree like structure is generated by a lack of stabilizer, allowing lateral growth and thus decreasing the density of morphological boundaries and consequently, the hardness.

Scratch tests were used in order to estimate the adhesion of the deposits under external solicitations. Table 2 presents the adhesion test critical load (*Lc*) in electroless plated NiB systems, obtained through the scratch test. These results referring to the first damage, for all coatings, were obtained by a combination of acoustic emission and microscopy observations. The damage features were determined by observation of the residual scratch, as shown in Fig. 6.

The first thing that can be observed from Table 2 is that the critical load for the first damage varies depending on the type of coating, with similar values for TcA and TcB and an inferior value for TcC. The damage appears from 18 N on TcC and the critical loads increase to 28 N for TcA and to 30 N for TcB. The highest value was obtained for TcB, which was quite impressive. The achieved value shows the superior adhesion of these coatings when compared with NiP coatings and with NiB-Pb [21,51].

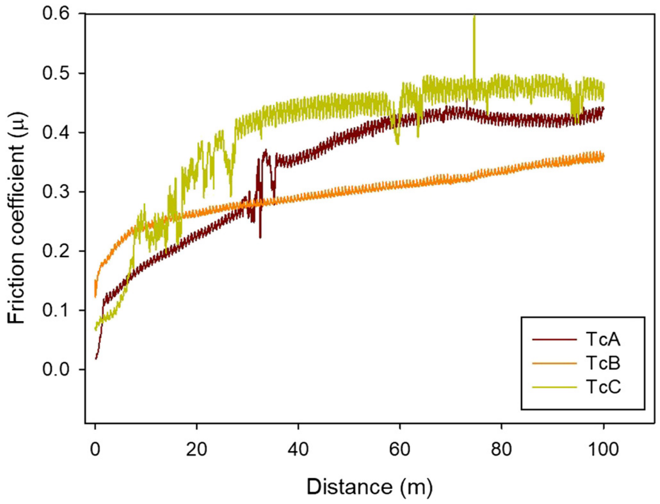

Fig. 7. Friction coefficient evolution of NiB-Sn samples.

The type of the first damage is similar for all types of coating. The first damage presented in all the cases is chevron cracks at the edge of the scratch. Shortly thereafter all the coatings presented transverse tensile cracking, this damage appearing at 32 N for TcA, 36 N for TcB and 28 N for TcC. It is important to note that all these failure modes are linked to cohesive failure, which is expected because these systems are constituted of coatings much harder than their substrate [21]. Coating TcC presented chipping for loads higher than 85 N. This fact in addition to the low critical load obtained for this coating suggests a low adhesion of TcC when compared to the other two coatings.

In general, these tests are indicative of good adhesion and scratch resistance and none of the coatings tested presented complete failure or scaling.

The friction coefficient indicates the ease of sliding between two

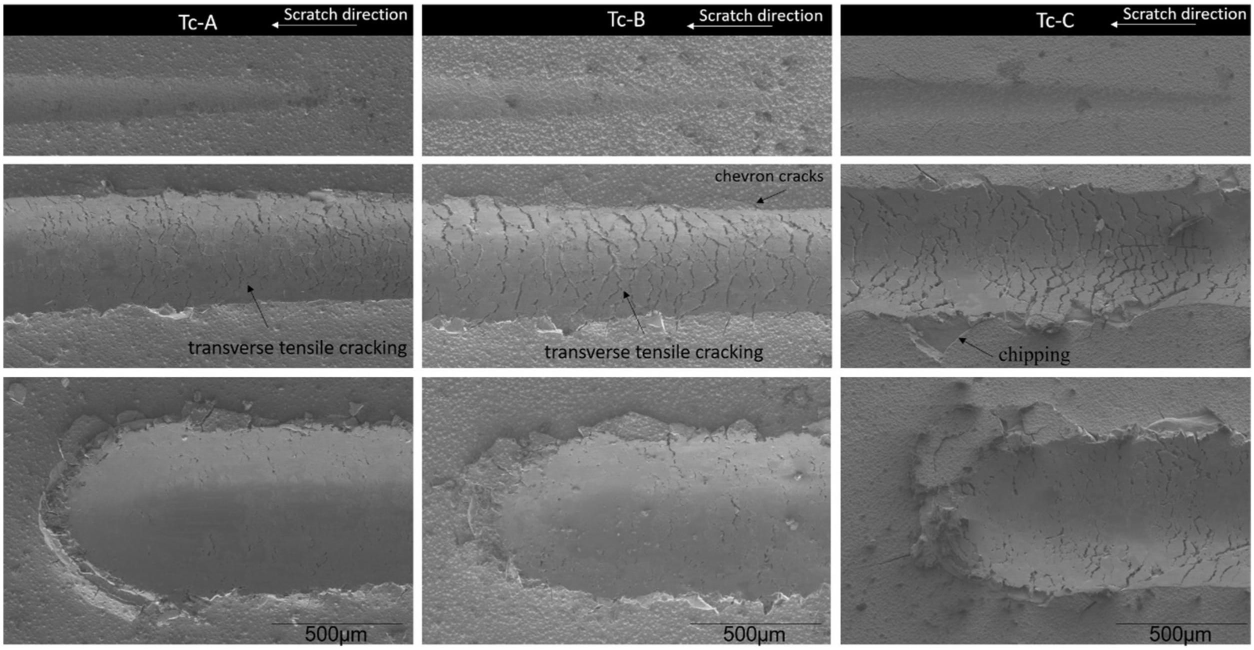

Fig. 6. Electroless NiB-Sn scratched coating surface: (a) TcA, (b) TcB and (c) TcC.

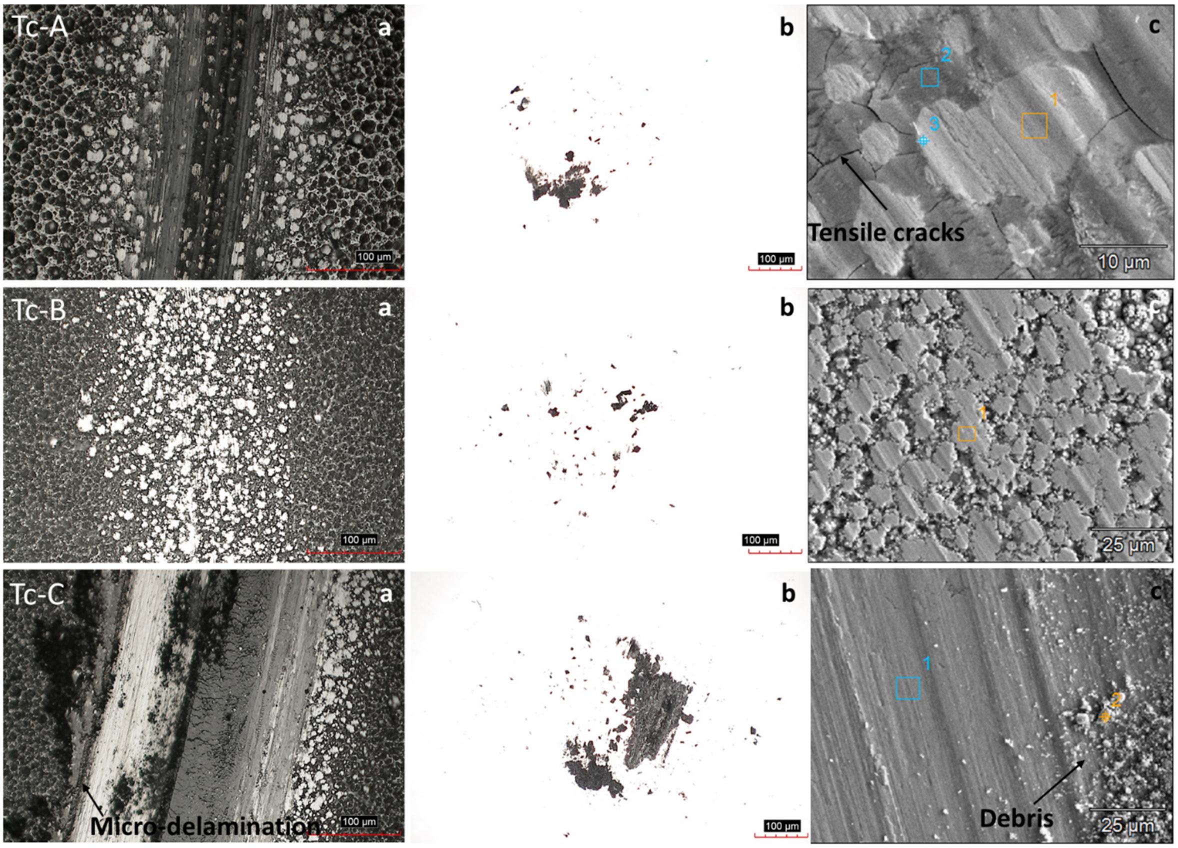

Fig. 8. Sliding wear tracks on the electroless NiB-Sn coatings TcA, TcB and TcC: (a) sliding wear tracks, (b) alumina ball surface after test, (c) debris particles and wear tracks grooves.

surfaces. As one can perceive in Table 2, the coefficient of friction varies depending on the type of coating, with a high value for TcC (0.51), followed by TcA (0.42), and an impressive small value for TcB (0.35). The friction coefficient for these kinds of samples varies with the distance and the results presented here are obtained at 100 m the friction coefficient evolution is show in the Fig. 7. Due to the high roughness TcA, needs more than 40 m to stabilize the friction coefficient, TcB has a constant increase until 100 m showing stabilization is still not reached: on the top of the columns is submitted to wear. TcC was a noisy curve due the lower adhesion of this coating and micro-delamination.

The specific wear rate (Ws) was calculated following the European standard EN 1017-13:2008, where Ws is the volume wear loss ΔV divided by the applied load F_N and the sliding distance S. The best wear behaviors are associated with lower values of Ws.

Assuming that the wear resistance is related to hardness and adhesion, one might suppose that the tribological behavior of samples TcB would be superior when compared to the other two samples. The worst behavior was presented by the sample TcC (Ws equal to 1.29 $\mu m^2/N$). Although this coating presented high hardness, its adhesion was lower when compared to the others and it presented chipping in some areas.

Further analysis carried out on the worn surfaces of the coatings after the pin-on-disk test was performed by means of electronic microscope (Fig. 8) and it shows how wear of columnar structure influences the tribological properties. In the case of TcA, as can be seen on Fig. 4, the top of a column is far from the top of the neighboring column, during the first moments of pin-on-disc test, the contact surface is too low and in consequence the pressure on a single column top is too high. This phenomenon generates tensile crack formation around the column. In addition, due the high height of the columns the region around the column does not play a role in wear resistance. However the repetitive effort heats the surface, generating the oxidation of these regions, as can be seen in Table 3. Surface analysis of the ball counterpart is in accord with the worn surface, just a small amount of material is removed, and the oxidized surface stay stuck to the substrate, so only minor regions of the ball presents coatings adhesion.

Table 3
Surface composition of coatings after wear test.

Wt%	C	O	Al	Ni	Sn
TcA - 1	0.8 ± 0.3	3.2 ± 0.5		93.0 ± 3.6	3.0 ± 0.5
TcA - 2	0.8 ± 0.2	37.4 ± 0.7	0.6 ± 0.1	59.7 ± 2.9	1.6 ± 0.4
TcA - 3	2.2 ± 0.3	17.1 ± 0.7		78.8 ± 2.8	1.9 ± 0.4
TcB - 1	1.0 ± 0.3	16.0 ± 0.7	0.6 ± 0.2	78.2 ± 3.1	4.2 ± 1.1
TcC - 1	0.5 ± 0.2		0.6 ± 0.1	96.7 ± 1.7	2.1 ± 0.3
TcC - 2	0.9 ± 0.4	16.8 ± 0.7	0.6 ± 0.2	79.1 ± 1.8	2.6 ± 0.3

TcB has an impressive tribological resistance when submitted to pin-on-disc test. This behavior can be explained once more by the columnar structure [52–54]. The size and distance between different columns in the TcB structure are responsible for a decrease in the contact area, that generates a decrease in the friction coefficient and in the total wear, however at the same time columns are sufficient dense to share the total load and resist the test. As can be seen in Fig. 8, only grooves from abrasive wear are observed in the worn surface. The composition analysis (Table 3) shows surface oxidation due to the heating caused by the wear test. Adhesion between ball and coatings is minor.

Due the lower adhesion, TcC is the only coating that presents materials in the worn borders. Micro delamination can be observed in the worn surface edges, in addition, a large formation of debris can be observed on the abrasive grooves. The ball analysis shows an adhesion phenomenon between the ball and the debris. The composition analysis after wear test (Table 3) shows that the coating surface is easily scratched before have time to heat and form oxides, just the debris particles

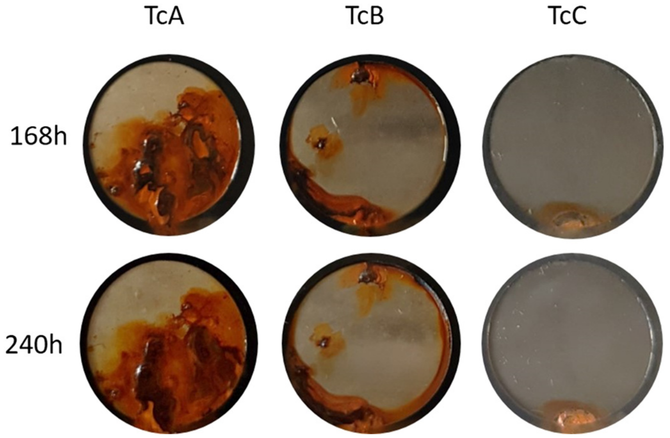

Fig. 9. Surface aspect of electroless NiB-Sn 15 ± 1 µm coatings after 168 h and 240 h salts spray.

are oxidized.

In conclusion, the three coatings presented similar mechanisms of abrasive and adhesive wear, due to the combination of high hardness and ductility, with abrasive wear as the predominant wear phenomenon. However, the adhesion and columnar morphology seems to have a large influence on the wear behavior. Similar wear mechanisms have been reported for other electroless nickel coatings in the literature [12,19,20,42–44].

3.2.3. Corrosion

With the aim of characterizing the corrosion properties, neutral salt spray test was carried out according to ASTM B117-07. There was no noticeable corrosion pits on the surface of the mild steel-coated samples until 48 h, after which the TcA and TcB samples started to corrode. TcC started to corrode after 72 h. For the bare mild steel, corrosion started after 1 h and the surface was completely corroded after 8 h [55]. The aspect of coated samples after 168 and 240 h of salt spray exposure is shown on Fig. 9. After 7 days (168 h) in neutral salt spray, the NiB-Sn samples presented a proportion of corroded surface varying between 62.2% for TcA and only 4.5% for TcC, with a value of 14.6% for TcB. After 3 more days of exposure, the corroded surface increases to 66.6%, 6.4% and 17.6% respectively (Table 5). All the coatings improve the corrosion behavior of mild steel. However, significant difference is obtained for the different concentrations of tin. As observed for the other coatings, the time before initiation of local corrosion and the percentage of corroded surface are affected by surface conditions, which explains the fact that smoother samples present the best behavior. On the other hand, the differences are really significant and can be affected by other factors. The analysis of the surface composition, Fig. 3, of the three different coatings shows that when compared with TcA and TcB, TcC presents 4 and 20 times more Sn, at the surface, respectively. Sn is known for its corrosion protective properties [56,57]. In addition, the analysis of Pourbaix (E-pH) diagrams [58,59], shows that at neutral pH (between 4 and 10), precipitation of $Sn(OH)_2$, that is a protective and stable hydroxide, occurs. One possible explanation for the high resistance of TcC can be the fact that nickel dissolution generates a high concentration on Sn atoms at the surface and then the precipitation of $Sn(OH)_2$ protects the coating surface. A similar mechanism is used to explain the high corrosion resistance of NiP samples [36,37].

Table 4
Corroded surface percentage after 168 and 240 h in neutral salt spray.

	Corroded surface % after 168 h	Corroded surface % after 240 h
TcA	62.2	66.6
TcB	14.6	17.6
TcC	4.5	6.4

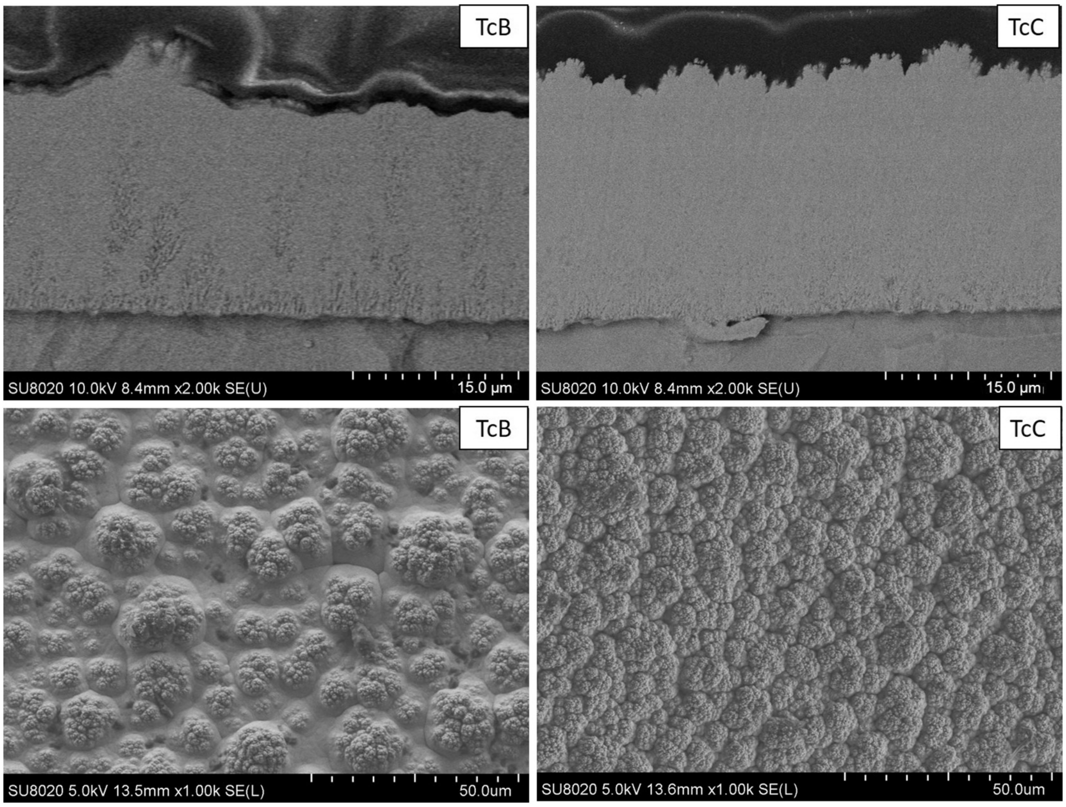

Fig. 10. SEM cross-section and surface morphology of ultrasound assisted NiB-Sn.

Table 5
Ultrasound assisted NiB-Sn properties.

	TcB	TcC
Thickness (μm)	21.8 ± 0.5	22.1 ± 0.4
Cross-section hardness hk_{50}	831 ± 32	845 ± 43
Roughness Ra (μm)	0.55 ± 0.05	0.34 ± 0.08

3.2.4. Ultrasound assisted NiB-Sn coatings properties

A preliminary characterization of ultrasound assisted (35 kHz frequency and 0.072 W/cm3 power) NiB-Sn samples was also realized. TcA is not characterized as this bath is not stable under those agitation conditions, ultrasound agitation is known in the literature by cause destabilization in electroless baths [60,61]. Fig. 10 shows the surface and cross-section morphology of the coatings. Changes in the morphology are limited; the tree like structure is present once more in the case of TcB and TcC presents fine columns. Surface morphology presents a slightly less texturized aspect, that is confirmed by the decrease in the roughness value (Table 4). However, once more, changes are minor.

A 20% increase is observed in the coatings thickness of TcB for one-hour deposition. Ultrasound assisted coatings are 21.8 μm thick after 60 min of plating. In The case of TcC, the increase is less representative, 6%, generating a 22,1 μm thick coating after 60 min of plating, this fact can be explained by the high stability of this baths [62] and the already very high deposition rate of these coatings with mechanical agitation.

Finally, hardness values are not influenced by ultrasound agitation in this case.

4. Conclusion

Electroless NiB-Sn plating was investigated in this study, as an alternative to NiB-Pb and NiB-Tl coatings, with the aim of combining the good wear resistance, high hardness and adhesion of traditional NiB coatings with a new environmentally friendly bath stabilized by Tin. These coatings could meet the ELV 2000/53/EC [38] and the RoHS 2002/95/EC [39] compliance.

The stabilizer properties of Tin chloride were investigated and proven. The properties of three different concentrations were characterized. When compared with the classical bath (NiB-Pb), the NiB-Sn one presents modified chemical composition, growth mode, morphology and mechanical properties.

The morphological features of the tin chloride stabilized coatings are modified depending on the stabilizer concentration. A finer cauliflower structure is reached with the increase of stabilizer concentration. The high concentration of stabilizer generates a more homogeneous thickness and less rough coatings.

The hardness of the two systems with high stabilizer concentration (TcB and TcC) is in the same range as that of NiB-Pb coatings. TcB also presents a scratch test resistance comparable to that presented by NiB-Pb coatings and a superior wear behavior. The corrosion results showed an impressive resistance in the case of high Sn concentration. In addition, ultrasound agitation generates just minor changes in the coatings properties.

The characterization showed that the TcB sample (0.1 g/L of $SnCl_2$), is the best candidate to replace NiB-Pb coatings, although an optimization of the roughness of this coating should be envisaged for some applications, ultrasound assistance with specific frequency and power could decrease be used. An additional introduction of Sn in the end of the deposition could increase the Sn concentration in the surface and generate better corrosion behavior.

Acknowledgments

The authors would like to thank Mr. Enrique Juste from BCRC (Mons, Belgium) for his help with the realization of the scratch tests. In addition, the authors would like to thank Dr.Sofia Gaiaschi from HORIBA Scientific (Palaiseau, France) for his help with the realization of the GDOES analyses. One of the authors (L. Bonin) wishes to thank the CNPq (Conselho Nacional de Desenvolvimento Científico e Tecnológico) for funding.

References

[1] B.N.G.K.I. Popov, S.S. Djokic, Metal Deposition Without an External Current, Kluwer academic publishers, New york, 2002.

[2] M. Scliesinger, Electroless depostion of nickel, in: M.P. Mordechay Schlesinger (Ed.), Mod. Electroplat, 5th ed., The Electrochemical Society Series, 2010, https://doi.org/10.1149/1.2425993.

[3] W.H. Safranek, J.B.H. Glenn O. Mallory (Ed.), Electroless Cobalt and Cobalt Alloys Section, American electroplaters and surface finishing society, New york, 1990, pp. 463–509.

[4] W. Riedel, Electroless nickel plating riedel, W ASM International: Metals Park, OH, 1991 ASTM International, Metals Park, OH, 1991.

[5] B. Zhang, Mechanism of electroless plating, in: Chemical Industry Press (Ed.), Amorph. Nano Alloy. Electroless Depos, Elsevier Inc., Amsterdam, Netherlands, 2016, pp. 583–627, , https://doi.org/10.1016/B978-0-12-802685-4.00010-8.

[6] R. Hu, Y. Su, H. Liu, Deposition behaviour of nickel phosphorus coating on magnesium alloy in a weak corrosive electroless nickel plating bath, J. Alloys Compd. 658 (2016) 555–560, https://doi.org/10.1016/j.jallcom.2015.10.300.

[7] Y. Gan, D. Chen, Z. Kang, A highly anticorrosive chromium-free conversion coating prepared on electroless Ni–P coating, Surf. Coat. Technol. 287 (2016) 25–32, https://doi.org/10.1016/j.surfcoat.2015.12.080.

[8] W. Wang, W. Zhang, Y. Wang, N. Mitsuzak, Z. Chen, Ductile electroless Ni–P coating onto flexible printed circuit board, Appl. Surf. Sci. 367 (2016) 528–532.

[9] A.S. Hamada, P. Sahu, D.A. Porter, Indentation property and corrosion resistance of electroless nickel-phosphorus coatings deposited on austenitic high-Mn TWIP steel, Appl. Surf. Sci. 356 (2015) 1–8, https://doi.org/10.1016/j.apsusc.2015.07.153.

[10] D. Seifzadeh, P. Shoghi, Electroless Ni-P/nano-WO3 coating and its mechanical and corrosion protection properties, J. Alloys Compd. 769 (2018) 149–160, https://doi.org/10.1016/j.jallcom.2018.07.304.

[11] F. Madah, C. Dehghanian, A.A. Amadeh, Investigations on the wear mechanisms of electroless Ni-B coating during dry sliding and endurance life of the worn surfaces, Surf. Coat. Technol. 282 (2015) 6–15, https://doi.org/10.1016/j.surfcoat.2015.09.003.

[12] I. Baskaran, R. Sakthi Kumar, T.S.N. Sankara Narayanan, A. Stephen, Formation of electroless Ni-B coatings using low temperature bath and evaluation of their characteristic properties, Surf. Coat. Technol. 200 (2006) 6888–6894, https://doi.org/10.1016/j.surfcoat.2005.10.013.

[13] K. Krishnaveni, T.S.N. Sankara Narayanan, S.K. Seshadri, Electroless Ni-B coatings: preparation and evaluation of hardness and wear resistance, Surf. Coat. Technol. 190 (2005) 115–121, https://doi.org/10.1016/j.surfcoat.2004.01.038.

[14] M. Anik, E. Körpe, E. Şen, Effect of coating bath composition on the properties of electroless nickel-boron films, Surf. Coat. Technol. 202 (2008) 1718–1727, https://doi.org/10.1016/j.surfcoat.2007.07.031.

[15] A. Mukhopadhyay, T.K. Barman, Effects of heat treatment on tribological behavior of electroless Ni–B coating at elevated temperatures, Surf. Rev. Lett. 25 (2018) 1–22, https://doi.org/10.1142/S0218625X18500142.

[16] C.A. Garcia-Aguirre, C. Dominguez-Rios, R. Torres-Sanchez, M. Roman-Aguirre, J.T. Holguin-Momaca, A. Aguilar-Elguezabal, Microstructure and transmission electron microscopy characterization of electroless Ni-B thin films deposited on MWCNTs, Surf. Coat. Technol. 282 (2015) 107–114, https://doi.org/10.1016/j.surfcoat.2015.10.023.

[17] J. Sudagar, J. Lian, W. Sha, Electroless nickel, alloy, composite and nano coatings - a critical review, J. Alloys Compd. 571 (2013) 183–204, https://doi.org/10.1016/j.jallcom.2013.03.107.

[18] K. Krishnaveni, T.S.N. Sankara Narayanan, S.K. Seshadri, Electrodeposited Ni-B coatings: formation and evaluation of hardness and wear resistance, Mater. Chem. Phys. 99 (2006) 300–308, https://doi.org/10.1016/j.matchemphys.2005.10.028.

[19] V.K. Bulasara, R. Uppaluri, M.K. Purkait, Effect of ultrasound on the performance of nickel hydrazine electroless plating baths, Mater. Manuf. Process. 27 (2012) 201–206, https://doi.org/10.1080/10426914.2011.566663.

[20] E. Ramírez-meneses, A.M. Torres-huerta, M.A. Domínguez-crespo, Synthesis and electrochemical characterization of Ni nanoparticles by hydrazine reduction using hydroxyethyl cellulose as capping agent, Electrochim. Acta 127 (2014) 228–238, https://doi.org/10.1016/j.electacta.2014.02.004.

[21] L.B.V. Vitry, Formation and characterization of multilayers borohydride and hypophosphite reduced electroless nickel deposits, Electrochim. Acta 243 (2017) 7–17, https://doi.org/10.1016/S0925-8388(03)00680-7.

[22] V. Vitry, L. Bonin, Increase of boron content in electroless nickel-boron coating by modi fi cation of plating conditions, Surf. Coat. Technol. 311 (2017) 164–171, https://doi.org/10.1016/j.surfcoat.2017.01.009.

[23] F. Delaunois, J.P. Petitjean, M. Jacob-Dulière, P. Liénard, P. Lienard, M. Jacob-Duliere, Autocatalytic electroless nickel-boron plating on light alloys, Surf. Coat. Technol. 124 (2000) 201–209, https://doi.org/10.1016/S0257-8972(99)00621-0.

[24] Y. Liang, Y.S. Li, Q.Y. Yu, Y.X. Zhang, W. jie Zhao, Z.X. Zeng, Structure and wear resistance of high hardness Ni-B coatings as alternative for Cr coatings, Surf. Coat. Technol. 264 (2015) 80–86, https://doi.org/10.1016/j.surfcoat.2015.01.016.

[25] R.A. Shakoor, R. Kahraman, W. Gao, Y. Wang, Synthesis, characterization and applications of electroless Ni-B coatings-a review, Int. J. Electrochem. Sci. 11 (2016) 2486–2512.

[26] X. Yin, L. Hong, B.H. Chen, T.M. Ko, Modeling the stability of electroless plating bath - diffusion of nickel colloidal particles from the plating frontier, J. Colloid Interface Sci. 262 (2003) 89–96, https://doi.org/10.1016/S0021-9797(03)00191-7.

[27] W.J. Cheong, B.L. Luan, D.W. Shoesmith, The effects of stabilizers on the bath stability of electroless Ni deposition and the deposit, Appl. Surf. Sci. 229 (2004) 282–300, https://doi.org/10.1016/j.apsusc.2004.02.003.

[28] Z. Xiao, W. Wang, L. Ye, Y. Sha, S. Tu, Effect of Cd2+ as a stabilizer in the electroless nickel plating system, Surf. Coat. Technol. 202 (2008) 5008–5011, https://doi.org/10.1016/j.surfcoat.2008.05.002.

[29] I. Baskaran, T.S.N.S. Narayanan, A. Stephen, Effect of accelerators and stabilizers on the formation and characteristics of electroless Ni-P deposits, Mater. Chem. Phys. 99 (2006) 117–126, https://doi.org/10.1016/j.matchemphys.2005.10.001.

[30] X. Yin, L. Hong, B. Chen, Role of a Pb2+ stabilizer in the electroless nickel plating system : a theoretical exploration, J. Phys. Chem. B (2004) 10919–10929, https://doi.org/10.1021/jp036070k.

[31] I. N.Feldstein. Surface Technology, Stabilizer for composite electroless plating, US6306466B1, 2001.

[32] L. Bonin, N. Bains, V. Vitry, A.J. Cobley, Electroless Deposition of Nickel-Boron Coatings Using Low Frequency Ultrasonic Agitation: Effect of Ultrasonic Frequency on the Coatings, 77 (2017), pp. 61–68, https://doi.org/10.1016/j.ultras.2017.01.021.

[33] E. Bash, Theory and Practice of Metal Electrodeposition, Springer, New York, 2015, https://doi.org/10.1017/CBO9781107415324.004.

[34] G.O. Mallory, The fundamental aspects of electroless nickel plating, Electroless Plat. - Fundmentals Appl, American electroplaters and surface finishing society, New york, 1990, pp. 1–56.

[35] C. Chen, B. Chen, L. Hong, Role of Cu2+ as an additive in an electroless nickel-phosphorus plating system: a stabilizer or a codeposit? Chem. Mater. 18 (2006) 2959–2968, https://doi.org/10.1021/cm0527571.

[36] R.B. Diegle, N.R. Sorensen, An XPS investigation into the passivity of an amorphous Ni-20P alloy, J. Electrochem. Soc. 135 (1987), https://doi.org/10.1149/1.2095880.

[37] R. Gan, D. Wang, Z. Xie, L. He, Improving surface characteristic and corrosion inhibition of coating on Mg alloy by trace stannous (II) chloride, Corros. Sci. 123 (2017) 147–157, https://doi.org/10.1016/j.corsci.2017.04.018.

[38] EC, Directive 2000/53/EC of the European Parliament and of the Council of 18 September 2000 on end-of-life vehicles, Eur. Comm. 2137 (2000) (010.001-1-010.001-22), http://ec.europa.eu/environment/waste/elv/.

[39] Council of the European Union, DIRECTIVE 2002/95/EC OF THE EUROPEAN PARLIAMENT AND OF THE COUNCIL of 27 January 2003 on the restriction of the use of certain hazardous substances in electrical and electronic equipment, Off. J. Eur. Union L 37/19 (2003) (2003), https://doi.org/10.1016/j.jclepro.2010.02.014.

[40] F. Delaunois, P. Lienard, Heat treatments for electroless nickel–plating on aluminium alloys, Surf. Coat. Technol. 160 (2002) 239–248, https://doi.org/10.1016/S0257-8972(02)00415-2.

[41] B. DW., Electroless nickel plating, Surface Engineering, ASM Handb, 5 ASM international, 2002(Online).

[42] W. Ke, Development of Lead-Free Electroless Nickel Plating Systems and Metal Thin Films on Silicone and Nafion Membranes, National University of Singapore, 2008.

[43] E. Correa, A.A. Zuleta, L. Guerra, M.A. Gómez, J.G. Castaño, F. Echeverría, H. Liu, P. Skeldon, G.E. Thompson, Tribological behavior of electroless Ni-B coatings on magnesium and AZ91D alloy, Wear 305 (2013) 115–123, https://doi.org/10.1016/j.wear.2013.06.004.

[44] Q.L. Rao, G. Bi, Q.H. Lu, H.W. Wang, X.L. Fan, Microstructure evolution of electroless Ni-B film during its depositing process, Appl. Surf. Sci. 240 (2005) 28–33, https://doi.org/10.1016/j.apsusc.2004.07.059.

[45] G.O. Mallory, The electroless nickel plating bath: effect of variables on the process, Electroless Plating, Fundam. Appl, 2009, p. 69 (71; 72).

[46] S.K. Das, P. Sahoo, Tribological characteristics of electroless Ni-B coating and optimization of coating parameters using Taguchi based grey relational analysis, Mater. Des. 32 (2011) 2228–2238, https://doi.org/10.1016/j.matdes.2010.11.028.

[47] V. Vitry, F. Delaunois, Formation of borohydride-reduced nickel–boron coatings on various steel substrates, Appl. Surf. Sci. 359 (2015) 692–703, https://doi.org/10.1016/j.apsusc.2015.10.205.

[48] V. Vitry, A. Sens, F. Delaunois, Comparison of various electroless nickel coatings on steel: structure, hardness and abrasion resistance, Mater. Sci. Forum 783–786 (2014) 1405–1413, https://doi.org/10.4028/www.scientific.net/MSF.783-786.1405.

[49] J.N. Balaraju, A. Priyadarshi, V. Kumar, N.T. Manikandanath, P. Praveen Kumar, B. Ravisankar, Hardness and wear behaviour of electroless Ni–B coatings, Mater. Sci. Technol. (2016) 1–12, https://doi.org/10.1080/02670836.2015.1137683.

[50] H. Ogihara, K. Udagawa, T. Saji, Effect of boron content and crystalline structure on hardness in electrodeposited Ni-B alloy films, Surf. Coat. Technol. 206 (2012) 2933–2940, https://doi.org/10.1016/j.surfcoat.2011.12.025.

[51] L. Bonin, V. Vitry, Mechanical and wear characterization of electroless nickel mono and bilayers and high boron-mid phosphorus electroless nickel duplex coatings, Surf. Coat. Technol. 307 ((2016) 957–962, https://doi.org/10.1016/j.surfcoat.2016.10.021.

[52] E. Correa, A.A. Zuleta, L. Guerra, M.A. Gómez, J.G. Castaño, F. Echeverría, H. Liu, A. Baron-Wiecheć, T. Hashimoto, P. Skeldon, G.E. Thompson, Coating development during electroless Ni-B plating on magnesium and AZ91D alloy, Surf. Coat. Technol. 232 (2013) 784–794, https://doi.org/10.1016/j.surfcoat.2013.06.100.

[53] J. Diabb, A. Juarez-Hernandez, R. Colas, A.G. Castillo, E. Garcia-Sanchez, M.A.L. Hernandez-Rodriguez, Boron influence on wear resistance in nickel-based alloys, Wear 267 (2009) 550–555, https://doi.org/10.1016/j.wear.2008.12.046.

[54] J.M. Fildes, S.J. Meyers, C.P. Mulligan, R. Kilaparti, Evaluation of the wear and abrasion resistance of hard coatings by ball-on-three-disk test methods-a case study, Wear 302 (2013) 1040–1049, https://doi.org/10.1016/j.wear.2012.11.018.

[55] L. Bonin, V. Vitry, F. Delaunois, Corrosion behaviour of electroless high boron-mid phosphorous nickel duplex coatings in the as-plated and heat-treated states in NaCl, H2SO4, NaOH and Na2SO4 media, Mater. Chem. Phys. 208 (2018) 77–84, https://doi.org/10.1016/j.matchemphys.2017.12.030.

[56] L.C. Tsao, Effect of Sn addition on the corrosion behavior of Ti-7Cu-Sn cast alloys for biomedical applications, Mater. Sci. Eng. C 46 (2015) 246–252, https://doi.org/10.1016/j.msec.2014.10.037.

[57] H. Li, H. Yu, T. Zhou, B. Yin, S. Yin, Y. Zhang, Effect of tin on the corrosion behavior of sea-water corrosion-resisting steel, Mater. Des. 84 (2015) 1–9, https://doi.org/10.1016/j.matdes.2015.06.121.

[58] W.T. Thompson, M.H. Kaye, Pourbaix diagrams for multielement systems.pdf, (2000).

[59] D. Minzari Morten, S. Jellesen Per Møller Rajan Ambat, On the Electrochemical Migration Mechanism of Tin in Electronics, Corros. Sci. 53 (10) (October 2011) 3366–3379.

[60] A.J. Cobley, T.J. Mason, V. Saez, Review of effect of ultrasound on electroless plating process, Trans. Inst. Met. Finish. 89 (2011) 303–309, https://doi.org/10.1179/174591911X13170500147670.

[61] A. Araghi, M.H. Paydar, Electroless Deposition of Ni–P–B$_4$C Composite Coating on AZ91D Magnesium Alloy and Investigation on Its Wear and Corrosion Resistance, 31 (2010), pp. 3095–3099, https://doi.org/10.1016/j.matdes.2009.12.042.

[62] G.O. Mallory, The effects of ultrasonic irradiation on electroless nickel plating, Trans. IMF 56 (1978) 81–86, https://doi.org/10.1080/00202967.1978.11870458.